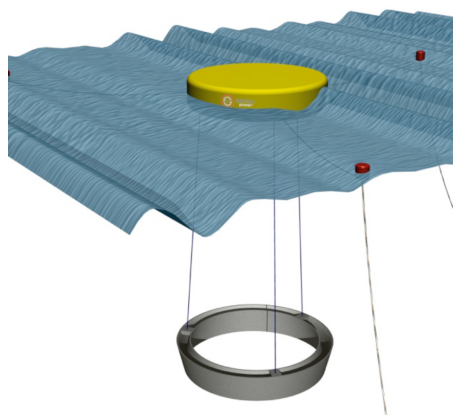


# Numerical and physical modeling of a flexibly-connected two-body wave energy converter

Brian J. Rosenberg\*  
Oscilla Power  
Seattle, WA, USA

Timothy R. Mundon  
Oscilla Power  
Seattle, WA, USA



**Figure 1: Triton WEC with original cylindrical surface float**

\*Corresponding author: rosenberg@oscillapower.com

This abstract details efforts to model and optimize the performance of Oscilla Power’s flexibly-connected, two-body Triton™ wave energy converter. A mid-fidelity numerical model is described that captures the essential dynamics and power take-out of the coupled system. Physical model experiments at scales of 1:60 and 1:50 are presented as a validation to the numerical results.

## 1. INTRODUCTION

The Triton wave energy converter (WEC) is a multi-modal two-body point absorber consisting of a surface float connected by three flexible tethers to a submerged heave plate (Figure 1). Mechanical energy is extracted from the environment in the form of wave-induced heave, pitch, and roll motion of the surface float through its reaction against a heave plate structure, which does not experience significant wave loadings due to its submergence depth. The resulting tension variation in each tether is transmitted to an independent linear power-

train, consisting of a linear hydraulic load transfer mechanism and a solid-state magnetostrictive [1], or other linear generator, housed inside the surface float.

The focus of the work described here is the development of an accurate numerical model of the Triton WEC and the use of this model to explore how changes to various parameters, such as the mass properties and hull geometry, can result in increased power capture.

## 2. NUMERICAL MODEL

In order to numerically model the performance of the system, a mid-fidelity time-domain model was developed in the commercial hydrodynamic code OrcaFlex. For the surface float, the frequency-dependent added mass, damping, and linearized excitation forces (Froude-Krylov and diffraction) were computed using the boundary element method solver NEMOH [2]. The submerged heave plate structure was represented by a simple Morrison formulation, and engineering estimates of the bulk added mass and drag coefficients, in translation and rotation, were informed from literature review (see for example [3]). Ongoing work at OPI is focused on more precisely measuring these coefficients through a combination of plunging experiments [4] and computational fluid dynamics.

The three connecting tethers between the heave plate and surface float were modeled using a finite-element method, in which the lines are represented as a number of segmented lumped masses. The power take out element (PTO) was modeled by three linear spring-damper elements (‘links’ in OrcaFlex) that were connected between the surface float and each tether.

## 3. PHYSICAL MODEL

In order to calibrate and validate the numerical models discussed, OPI constructed and tested two Froude scaled physical models of the Triton WEC at 1:60 and 1:50 scale. The 1:60 scale model included a cylindrical surface float, while the 1:50 scale model included an improved surface float shape, shown in Figure 2, that is discussed further in Section 5.

Both physical models included representative power take-out (PTO) using the same general mechanism. To

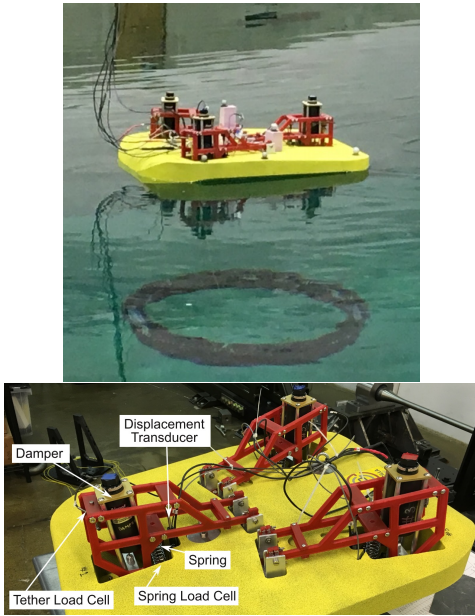


**Figure 2: 1:50 scale physical model showing the representative PTO arrangement.**

accurately represent the PTO, a spring-damper assembly was mounted to the surface float at each tether location, as shown in the lower image in Figure 2. Changes in the tether tension, as a result of wave-float interaction, cause each arm to oscillate about its pivot point. The difference between the tether force and the restoring spring force, accounting for the arm kinematics at each location, represents the force transmitted the damper (a tunable air dashpot). The dissipated power was measured using this damping force multiplied by the velocity measured from a displacement transducer. In addition to the PTO instrumentation, the translations and rotations of the surface float were measured using Qualisys motion capture cameras in both models.

#### 4. MODEL VALIDATION

As a first step in validating the physical model results against the numerical results, the wave/structure interaction with the surface float, calculated by the linear potential flow solver, was first considered. Response amplitude operator (RAO) analysis was used to look at the frequency response of an isolated surface float. Figure 3 shows the translational and rotational motion of the cylindrical surface float as a function of wave period. In both the physical model tests and the OrcaFlex simulations, the RAO profiles were generated from a white noise wave input. Also shown for comparison are regular wave results from the WEC-Sim code [5], demonstrating excellent agreement.

The lower plot in figure 3 shows the motion RAO of the cylindrical surface float when connected to the heave plate in a full-system configuration, comparing experiments to the numerical simulations. The vertical dashed lines, which represent the natural heave and pitch periods from experimental decay tests, also align closely

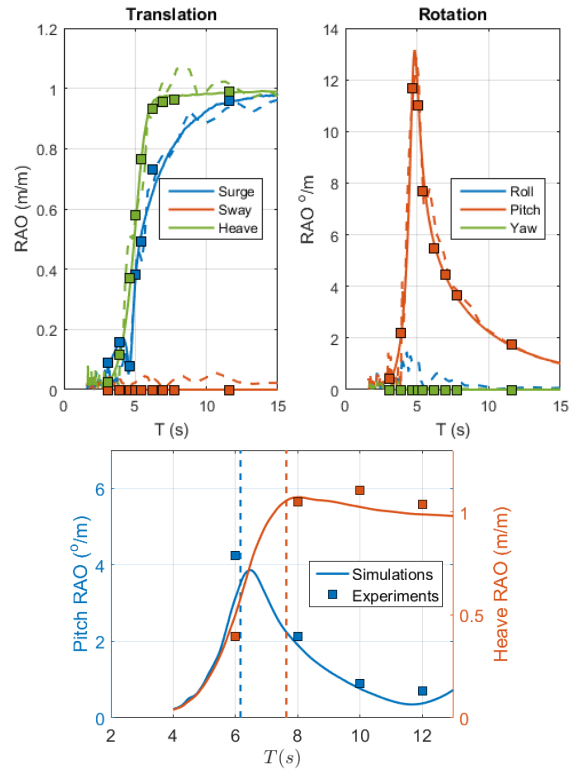


**Figure 3: TOP: Motion RAO of the cylindrical surface float in isolation (i.e. no heave plate). (---) 1:60 scale experiments (—) OrcaFlex model (□) WEC-Sim model. BOTTOM: Motion RAO of the cylindrical float when connected to the heave plate, compared to 1:60 experimental results**

with the RAO peaks predicted by the numerics. Furthermore but not shown here, the tether tensions and power capture were also reasonably well-captured by the numerical model to within 20%.

#### 5. DESIGN OPTIMIZATION

The relatively modest computational time of the OrcaFlex model (approximately 1 hour on a desktop computer for a full-scale device undergoing 1 hour of irregular waves) allows many different device configurations to be considered in the optimization.

##### 5.1 Mass properties

The first optimization performed was on the global mass properties of the two-body system. For a fixed total system mass, Figure 4 demonstrates the effect of distributing the mass differently between the heave plate and surface float, with a mass ratio  $M_{float}/M_{heaveplate}$  ranging from 0.54 to 1.7. Each contour level represents the effective wideband power capture of the system, black being the highest and white being the lowest, with the red circle denoting the highest power configuration. The results suggest that a float to heave plate mass ratio slightly less than 1 is optimal.

In addition to the system mass distribution, the mo-

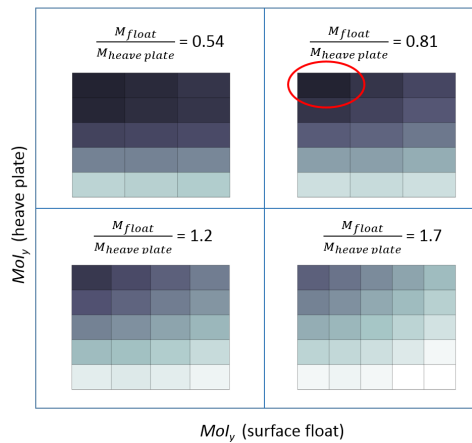


Figure 4: Contours of wide-band power capture for different mass distributions and moments of inertia for the surface float and heave plate. Surface float  $MOI_y \in [2 \times 10^4, 2 \times 10^5] Te \cdot m^2$  and heave plate  $MOI_y \in [7 \times 10^4, 2 \times 10^5] Te \cdot m^2$ .

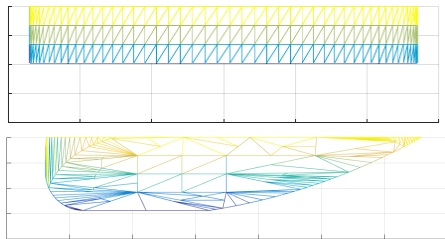


Figure 5: Underwater profile of the cylindrical (TOP) and asymmetric (BOTTOM) surface float. Waves propagate right to left.

ment of inertia (MoI) balance between the two bodies is important parameter in terms of power capture from pitch motion. Our numerical results suggest that a low surface float to heave plate MoI ratio maximizes capture, consistent with earlier findings [1]. Conceptually, this makes sense as a reaction structure with a large MoI has a large inertial resistance to rotation and therefore creates stronger reaction forces in the tethers.

## 5.2 Surface float shape

To obtain improved performance compared to a cylindrical surface float, an asymmetric profile that radiates predominantly in the incident wave direction was investigated. A parametric study using NEMOH and OrcaFlex was performed to examine the effect of different bow and stern curvatures on the system wideband power capture, and the best float shape is pictured in Figure 5. We found numerically that moving the center of buoyancy slightly further behind the geometric center on the surface float (as a result of the altered lower stern radius and higher bow radius) significantly enhanced pitch motion and resultant power capture.

These numerical findings are corroborated by physical model tests that were conducted during 2015. Figure 6

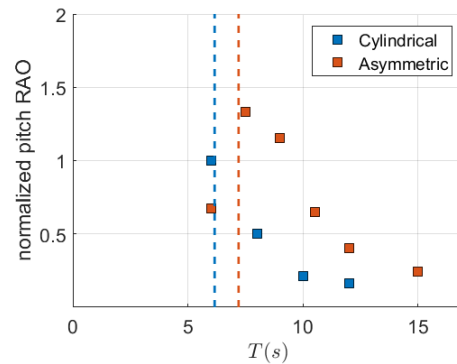


Figure 6: Pitch response of the two surface float designs (normalized with respect to the cylindrical shape) when connected to the heave plate and PTO

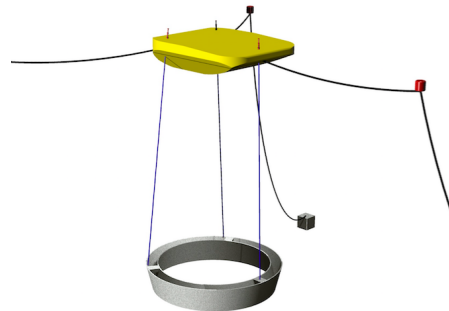


Figure 7: Triton WEC with optimized surface float

compares the surface float pitch RAO for the full system with cylindrical and asymmetric shapes (both Froude scaled to 1:1). At resonance, the asymmetric surface float design increases the pitch amplitude by approximately 35% and also creates a fuller response band. A Triton WEC with the improved asymmetric float design is shown in figure 7.

## 6. ACKNOWLEDGEMENT

Oscilla Power would like to thank HR Wallingford and the University of Maine Advanced Composites Center for assisting us in completing the physical model validation exercises, and its investors for the financial support that allowed this research to take place.

## 7. REFERENCES

- [1] Mundon, T., and Nair, B., 2014. "Optimization of a magnetostrictive wave energy converter". In Asian Wave and Tidal Energy Conference.
- [2] Babarit, A., and Delhommeau, G., 2015. "Theoretical and numerical aspects of the open source BEM solver NEMOH". In 11th European Wave and Tidal Energy Conference (EWTEC2015).

- [3] Brown, A., and Thomson, J., 2015. "Heave plate dynamics for a point absorbing wave energy converter". In the 3rd Marine Energy Technology symposium.
- [4] Li, J., Liu, S., Zhao, M., and Teng, B., 2013. "Experimental investigation of the hydrodynamic characteristics of heave plates using forced oscillation". *Ocean Engineering*, **66**, pp. 82–91.
- [5] Ruehl, K., Michelen, C., Kanner, S., Lawson, M., and Yu, Y.-H., 2014. "Preliminary verification and validation of WEC-Sim, an open-source wave energy converter design tool". In ASME 2014 33rd International Conference on Ocean, Offshore and Arctic Engineering, American Society of Mechanical Engineers, pp. V09BT09A040–V09BT09A040.